Aeroacoustics Conferences
30 May - 1 June, 2016, Lyon, France
22nd AIAA/CEAS Aeroacoustics Conference

A schlieren and nearfield acoustic based experimental investigation of screech noise sources

Bertrand Mercier*
Laboratoire de Mécanique des Fluides et dAcoustique
UMR CNRS 5509, École Centrale de Lyon, 36 Av. Guy de Collongue, 69134 Écully, France

Thomas Castelain†
Univ Lyon, Université Lyon 1
LMFA UMR CNRS 5509, 36 av. Guy de Collongue, 69134 Écully Cedex, France

Christophe Bailly‡
Laboratoire de Mécanique des Fluides et dAcoustique
UMR CNRS 5509, École Centrale de Lyon, 36 Av. Guy de Collongue, 69134 Écully, France

A series of experiments coupling high speed schlieren visualizations and near field acoustic investigations of three underexpanded jets are used to determine the screech acoustic source location. The jets exhibit screech tones of mode A1, A2, and B when the exhaust conditions correspond to the perfectly expanded jet Mach numbers M_j equal to 1.13, 1.15, and 1.35. The source was sought at a shock tip, the fourth shock is most likely found to radiate screech associated acoustic feedback for all modes. This is deduced from nearfield phase measurements. Complementary, high-speed schlieren movies help in estimating the convection velocity of screech associated hydrodynamic structures. From this analysis, the duration of the whole screech loop is found to consist of four periods of screech for modes A1 and B, and five periods for mode A2.

Nomenclature

D	Nozzle diameter, mm
k_h	wave-number of the hydrodynamic instability, m^{-1}
k_s	wave-number of the acoustic wave, m^{-1}
k_{sw}	wave-number of the standing wave, m^{-1}
M_j	Fully expanded jet Mach number
NPR	Nozzle Pressure Ratio
p	Amplitude of the phase averaged nearfield acoustic wave
R	Cross correlation function
r	Radial distance, mm
Re_j	Reynolds number based on nozzle diameter
s	Time history of a pixel in schlieren film
$\bar{S}$	Time averaged of s
S^c	Coherent component of s
S''	Turbulent component of s
St_s	Strouhal number of the screech frequency based on nozzle diameter

*PhD Student, École Centrale de Lyon, bertrand.mercier@doctorant.ec-lyon.fr.
†Assistant Professor, Université Lyon 1
‡Professor, École Centrale de Lyon,Senior Member

t	time
T_s	Screech period
U_c	Convective velocity, m/s
U_j	Fully expanded jet velocity, m/s
V_p	Phase velocity, m/s
z	Longitudinal coordinate, mm
$z_{4^{th}}$	Longitudinal coordinate of the fourth shock, mm
$\Delta\phi$	Phase difference regarding screech phenomenon, rad
λ_h	Hydrodynamic wavelength, m
λ_s	Acoustic wavelength, m
λ_{sw}	Standing wave wavelength, m
ϕ	Phase regarding screech phenomenon, rad
$\phi_{4^{th}}$	Phase at the fourth shock regarding screech phenomenon, rad
σ_s	Standard deviation of s

I. Introduction

The noise emitted by imperfectly expanded supersonic jet can be split up into mainly three components. They are generally referred to as the mixing noise, the broadband shock-associated noise and the screech. Although they have all been deeply investigated in various studies, our knowledge is still incomplete, and prediction remains dependent on empirical parameters. Tam's review on supersonic jet noise will provide further details on shock noise.[1] Screech phenomenon suffers in particular from a lack of quantitative experimental data including both the turbulent flow and the radiated sound field. The screech generation process is studied since 1950, and several different models have been established so explain the mechanism principle and predict the frequency. The existence of an array of sources expected to be the shocks was first mentioned by Powell.[2] But later, some schlieren observations led Powell *et al.*,[3] Umeda and Ishii[4] and Tam *et al.*[5] to state that only one source is involved in screech mechanism. Panda[6] pointed out a region in the near field between the third and fourth shock, upstream this limit acoustic waves propagate toward the nozzle, whereas, they go with the flow downstream. Such a behavior characterizes the location where acoustic waves are emitted. Raman[7] also experimentally investigated this source location on rectangular jet and figured out that the third shock is responsible for sound radiation at $M_j = 1.45$ and the fourth is involved at $M_j = 1.75$. The present study intends to provide reliable data on the location of this source within circular jets. In this purpose, the loop composed of the convected hydrodynamic instability wave followed by the upstream propagating acoustic feedback, is displayed in a graphical fashion allowing assessment of the loops consistency according to screech frequency. This assessment rests upon criterion on the ability for the loop to spend an integer number of screech periods. This is a necessary condition to make sure that a new hydrodynamic structure is triggered and so a new screech cycle start off. A second criterion to select the feedback source is to account only for those located at a shock tip. This is the most probable location according to numerical studies of shock leakage by Suzuki *et al.*,[8] Shariff and Manning,[9] or Berland *et al.*[10] It is shown that a moving shock is a source of compression and expansion waves that are normally internally reflected, but that can leak if some requirements on the vorticity in the shear layer are met, especially for large vortical structures, thus if coherent structures are developed enough. This analysis will assume the speed of sound constant while traveling in the jet vicinity, and there is no account for non-linear effects. No similar assumption is made for hydrodynamic convective velocity, that are directly estimated from measurement. Near field acoustic measurements on longitudinally and transversally microphone will also take part of the analysis.

The present experimental study is carried out from investigations of three different setting points of under-expanded jet through schlieren visualization apparatus. Two of these points were measured by André *et al.* with a rig which has already been discussed in André *et al.*,[11,12] but for the purpose of this study near field acoustic investigation were required, as a consequence the experimental rig was set up again. Note also that the present analysis of the time-resolved schlieren data is original.

Considered cases are nozzle pressure ratio NPR = 2.23, 2.27, 2.97 that correspond to perfectly expanded jets exhausting at $M_j = 1.13$, 1.15, 1.35, which respectively turn into a A1, A2, and B screech mode. The table 1 summarizes the test conditions. The case $M_j = 1.13$ was measured during the last test campaign.

M_j	NPR	f_s (Hz)	St_s	Mode	U_j (m/s)	Re_j
1.13	2.23	5407	0.57	A1	350	1.23×10^6
1.15	2.27	6152	0.63	A2	355	1.27×10^6
1.35	2.97	3270	0.32	B	404	1.64×10^6

Tab. 1 Setting points of the study. $St_s = f_s D/U_j$, $Re_j = \rho_j U_j D/\mu$

The experimental set-up will be detailed in Section 1, the investigation of the screech associated phase velocity will be presented in Section 2, the estimation of the modulated convective velocity is analyzed in Section 3. Finally, in Section 4, the source location will be sorted out for all three modes after the confrontation of near field acoustic and eligible locations based on previously detailed criteria.

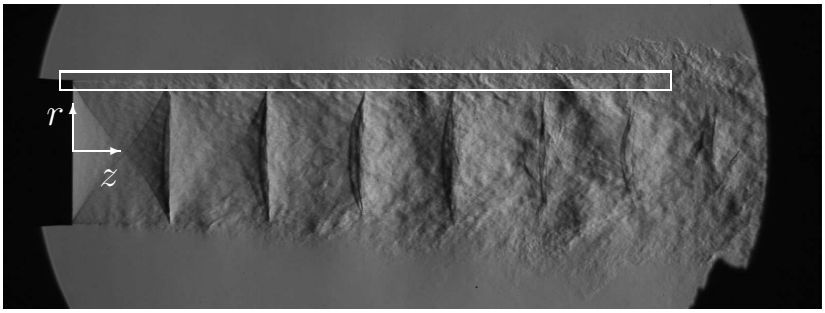

Fig. 1 Large field schlieren visualization of the $M_j = 1.15$ jet in which is represented the region used for acquisitions detailed in this study by a white rectangle. Jets flow from left to right. Exposure time is 4.2μs. The acquired field is bounded by $z/D \in [-0.05,\ 4.2]$ and $r/D \in [0.44,\ 0.54]$

II. Experimental set-up

Investigated jets are issued from a $D = 38$ mm diameter convergent nozzle with 0.5 mm thick lip. All the data were obtained in the supersonic wind tunnel that exhausts in the large anechoic chamber of Laboratoire de Mécanique des Fluides et d'Acoustique at Ecole Centrale de Lyon. The wind tunnel is fed in air by a centrifugal compressor driven by a control system ensuring stable total pressure with time. The measurement system is a conventional Z-type schlieren apparatus equipped with two f/8 parabolic mirrors of diameter 203 mm. It is lighted up by a 18 W array of four led LEDs mounted with a lens and a pinhole ensuring a better pinpoint like source. The knife-edge is set perpendicular to the jet axis, so it allows observation of axial density gradient. Schlieren visulations are recorded by a high speed CMOS camera. There is one record per jet and it results in 230,000 frames (520,000 frames for older records) of 24x1024 pixels (16x640 pixels for older records). The exposure time is 4 μs and the sample rate is 220,472 fps (1.8 μs and 430,769 fps for older records).

Each pixel of the film contains the record of a signal proportional to the axial density gradients sampled at 220.5 kHz over about 1 s. Attention has to be paid to the intrinsic integrating effect of schlieren visualisation, the measured density gradient is actually integrated over the whole light path between mirrors. This problem is partially overcome by the location of the field of view covered by the camera that has been chosen in the mixing layer to point out interaction between hydrodynamic and acoustic density field. This is also the most favorable region to avoid integration effects because the thickness of the jet crossed by light is the smallest. This probed region is delimited in the axial direction z by $z/D \in [-0.05,\ 4.5]$ ($z/D \in [-0.05,\ 4.2]$ for older records) and in the radial direction r by $r/D \in [0.44,\ 0.54]$. This domain is shown in figure 1 by a white rectangle drawn on an example of large field schlieren image for the $M_j = 1.15$ jet. This field of view covers the first six shocks for cases $M_j = 1.13$ and $M_j = 1.15$, but only the first three for the $M_j = 1.35$ case. Consequently, two films are recorded for this third case, one at the standard field range described above, and a second with the same dimension but shifted by two diameter long in the axial direction in order to

extend the studied region down to the fifth shock. The seek of this extended field of view justifies from the consensus that screech sound source is somehow contained within the first six shock cells. According to Umeda and Ishii,[4] sources exist in the first six cells and one seems to be dominant at the rear of the third shock cell for the C mode. Gao and Li situate that sound source at the fifth shock for A1, B and C modes.[13] Edgington-Mitchell *et al.*[14] investigated C mode, and suggested that acoustic waves are more likely to be emitted between the second and the fourth shock cell, wherein the coherent vorticity undergoes the largest fluctuations.

Since the data were not gathered in the exact same conditions, the first step was to ensure the agreement of old and new data sets. In this way screech frequency are compared in figure 2. A frequency slightly lower is found for A1, A2, and B modes in the last experiment, this discrepancy is the result of a difference in ambient temperature, the first set was measured in summer at an ambient temperature of 20°C instead of winter condition at 4°C.

The investigation consists in longitudinal and radial traverse with two 1/8" microphones as measurement devices. In both cases one microphone is kept steady to make a phase reference with respect to screech phenomenon, whereas a second one is moved by increment of about a tenth of the shock cell length from $z/D = 0$ to $z/D = 6.5$ or 8. Longitudinal investigations are operated at constant $r/D = 1$ from the lip line ($r/D = 1.5$ from the jet axis). Radial measurements are similar with the experiment carried out by Raman on rectangular jet,[7] the moving microphone is kept at constant $z = 0$ and moves from $r/D = 0.5$ to $r/D = 8$ by increments of 3 or 4 mm. Pressure signals are recorded simultaneously at 204.8 kHz.

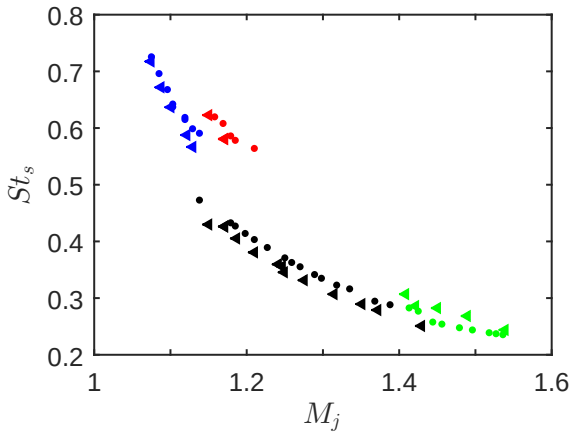

Fig. 2 Screech Strouhal number based on jet nozzle diameter D against perfectly expanded jet mach number. Triangles were measured in 2016, circles were measured in 2011 by André *et al.*;[15] ■ mode A1, ■ mode A2, ■ mode B, ■ mode b and C

III. Screech associated phase velocity

Wesltey and Wooley[16] have mapped the near field acoustic pressure by traversing a microphone in the jet vicinity, and have brought out a set of juxtaposed pressure nodes and antinodes synchronous with screech. They interpreted this observation as a standing wave pattern resulting from the interaction between the convected instability wave pressure field that leaks out from the mixing layer, and the upstream propagating acoustic pressure field.[17]

The full records are split up into the 24×1024 (16×640 for older records) time histories referred to as $s(z, r, t)$. Each of them contains the time history of the axial density gradient integrated over the light beam path. This axial density gradient is thus composed by the hydrodynamic contribution, and by the near field acoustic contribution. As previously shown by Wesltey and Wooley, when hydrodynamic and acoustic density fields are interacting, a quasi-standing wave pattern appears. This interaction also modulates the phase velocity of the resultant wave, and prevents from studying independently the acoustic from the hydrodynamic wave propagation. Panda[17] established a relation between the standing wave pattern, the instability wave-number and the acoustic wave-number respectively called k_{sw}, k_h and k_s. The resulting wave-number k_{sw} is then

given by

$$k_{sw} = k_h + k_s \tag{1}$$

A. Phase velocity estimation method

For the purpose of the study, the convection velocity of structures will have to be estimated in order to figure out the necessary time for the structures to travel within the shear layer. This convection velocity is expected to be the velocity around which the phase velocity of the resultant acoustic hydrodynamic interaction is modulated. The aim of measuring this phase velocity is then to assess the consistency of the estimated convective velocity.

The screech associated phenomena are found to be very strong, periodic, and stable. As a consequence the phase averaging method is a convenient approach to isolate screech related fluctuations from turbulence in the sense of Reynolds decomposition, in which the raw signal measured in the flow $s(z, r, t)$ can be split into a mean component $\overline{S(z, r)}$, a coherent component $S^c(z, r, \phi)$ and a turbulent component $S''(z, r, t)$ such that

$$s(z, r, t) = \overline{S(z, r)} + S^c(z, r, \phi) + S''(z, r, t) \tag{2}$$

Where $\phi(t)$ denotes the phase at time t in the screech cycle. Such a post-processing has already been tested for instance by Panda [6] and has provided consistent results. This treatment requires a reference signal that exhibits the features of the phenomenon to isolate, and that is in phase with the record. The ability to reject turbulence from coherent component of signal increases with the the magnitude of the signal to noise ratio at the region selected for probing the reference signal. The greatest signal to noise ratio is found in the region at rest right above the nozzle lip. There is no such a quiet area in the downstream shifted case at $M_j = 1.35$, the reference signal extracted from the upstream region of the field of view ($z/D = 1.7$) is found to perform well enough for the purpose of the present study, the result is noisy but still contains the wave features.

The reference signal is the average of the time histories of four adjoin pixels, it is then low-pass filtered. The cut-off frequency is set 20% above the screech frequency in order to guarantee that screech phenomenon is not filtered out even if it experiences jitter.

Time marks t_i are then determined to stand at the local maxima on the periodic reference signal, the time interval separating two marks is therefore the screech period T_{si} of this particular cycle. The phase ϕ of all frames can now be estimated according to their recording time t, and by assuming a linear evolution of the phase across the current period,

$$\phi(t) = 2\pi \frac{t - t_i}{T_{si}} \text{ for } \; t \in [t_i, \; t_{i+1}] \tag{3}$$

A phase resolution is then defined so as to discretise a period into bins, and to average all frames matching in phase with respect to this discretisation. For instance, results sorted out with bin width of $\pi/4$ are presented in figure 3 for all the three cases. The screech associated wave is clearly visible and travels downstream. Nevertheless, this wave is visible only further downstream a given limit long as about one to two shock cells. The relative long time of acquisition and high frequency sampling compared to screech time scale allows to reduce the phase resolution down to 8° without trouble of averaging convergence. The screech period is thus divided into 45 bins. Furthermore, the time averaged schlieren image computed from the full scope is subtracted to the phase averaged result in order to keep only the screech associated phenomena. An example of the result of this processing applied onto the lip line ($r = 0.5D$) is given in figure 4. The signals $S^c(z, r = 0.5D, \phi)$ of three of the forty five phase averaged frames, chosen equal to $\phi = 0$, $2\pi/3$, and $4\pi/3$, are plotted to illustrate the waveform of the screech associated wave at the given phase. In dashed line is also represented the low-pass filtered envelope of the wave, it defines the extreme value that the wave reach over one period at each z of the lip line. Note that signal amplitude is not scaled because this quantity is not relevant unless calibration process is performed and screech mode is asymmetric.

All forty five frames are then weakly low-pass filtered along axial direction to reject high wave-number oscillations, but to keep the wave form undamaged. The locations at which the wave crosses the zero amplitude line is recorded in parallel with the corresponding phase. When plotted in the plane ($z/D, \; \phi$), these sets of couple coordinates represent curves attached to a wavefront as in Westley and Wooley.[16] The curves are isolated one from the other, and their slope $dz/d\phi$ are estimated by a succession of linear regressions applied on ten following and overlapping points. This method performs better in those conditions than the

conventional finite-difference derivative calculation. The phase velocity V_p is then given by

$$V_p = \frac{2\pi}{T_s}\frac{dz}{d\phi} \tag{4}$$

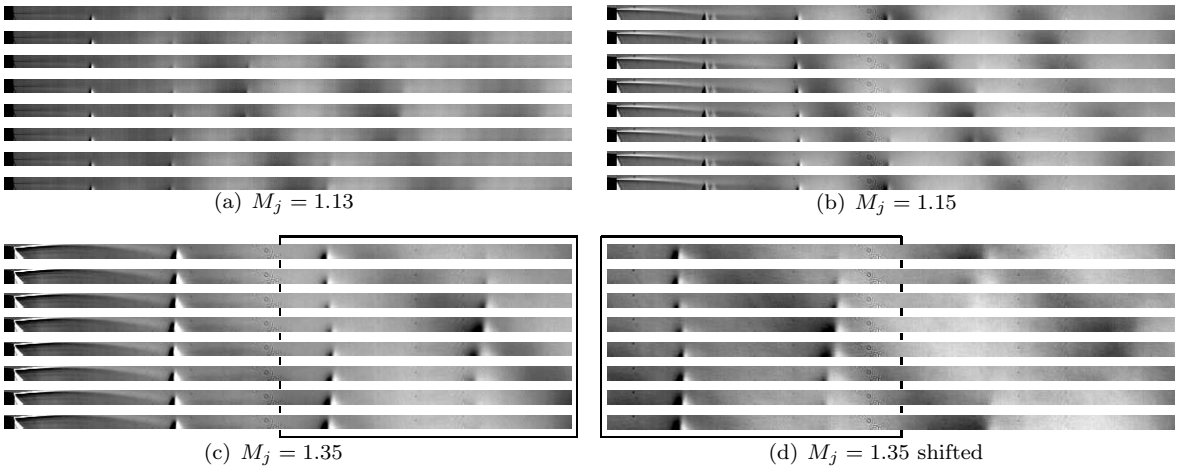

(a) $M_j = 1.13$ (b) $M_j = 1.15$ (c) $M_j = 1.35$ (d) $M_j = 1.35$ shifted

Fig. 3 Phase averaged schlieren visualization at screech frequency of the three jets at equi-spaced 8 phases $jT_s/8$ for $j = 0, \cdots, 7$. Jets flow form left to right. The field of view is delimited by $z/D \in [-0.05,\ 4.2]$ and $r/D \in [0.44,\ 0.54]$ for (a),(b),(c) and $z/D \in [1.9,\ 6.15]$ for (d). For the $M_j = 1.35$ cases, the two boxes mark out the region which is visible in the shifted and the unsifted field of views.

B. Phase velocity analysis

The phase velocity, extracted using the phase averaging method as described in the previous Section, is plotted for the three cases in figure 5. Each phase velocity estimation is displayed as a dot. The large amount of dots is the result of the high phase resolution. The robustness of the present method is sustained by the low scattering of all points. In all three cases, the phase velocity exhibits the modulated behavior explained by Panda[17] as the result of the interaction between the instability hydrodynamic wave convected downstream, and the acoustic wave propagating back to the nozzle. No phase velocity value is represented upstream the first shock, because in this region the phase velocity is negative, i.e. the resultant wave associated with screech is moving toward upstream. The exact location of this inversion is observable as a kind of node in figure 4 at $z/D = 0.93$ for $M_j = 1.13$, $z/D = 0.73$ for $M_j = 1.15$ and $z/D = 1.6$ for $M_j = 1.35$. Upstream this limit, the acoustic density field is stronger than hydrodynamic and downstream, hydrodynamic structures are amplified enough to become predominant. Hence, upstream this limit, the phase velocity is modulated by hydrodynamic around speed of sound, and downstream, acoustic modulates phase velocity around convective velocity.

It is possible to derive the convective velocity of screech associated structures from equation (1) if fs, C_0, and λ_{sw} are known. The screech frequency is measured, and the speed of sound in the surrounding of the jet can be determined from the ambient temperature. λ_{sw} might also be deduced since it is the phase velocity modulation wavelength in figure 3 and the envelope modulation wavelength in figure 5. Nevertheless, in these two methods, the difficulty is to properly identify the maxima and minima of the standing wave pattern, because of low wave-number variations along the z axis of both the envelope and phase velocity. therefore the estimation of λ_{sw} is biased. This approach to determine U_c is thus limited due to the lack of precision on λ_{sw}.[18] In the following, a direct mean to determine the convective velocity for the flow structures contributing to the screech is presented.

IV. Convective velocity of screech induced structures

The estimation of the convective velocity of the large coherent structures that play a role in the screech mechanism, is the first step to be able to predict the traveling time within the shear layer until they interact somehow with a jet feature such as shocks. Many attempts to measure this velocity have been carried out

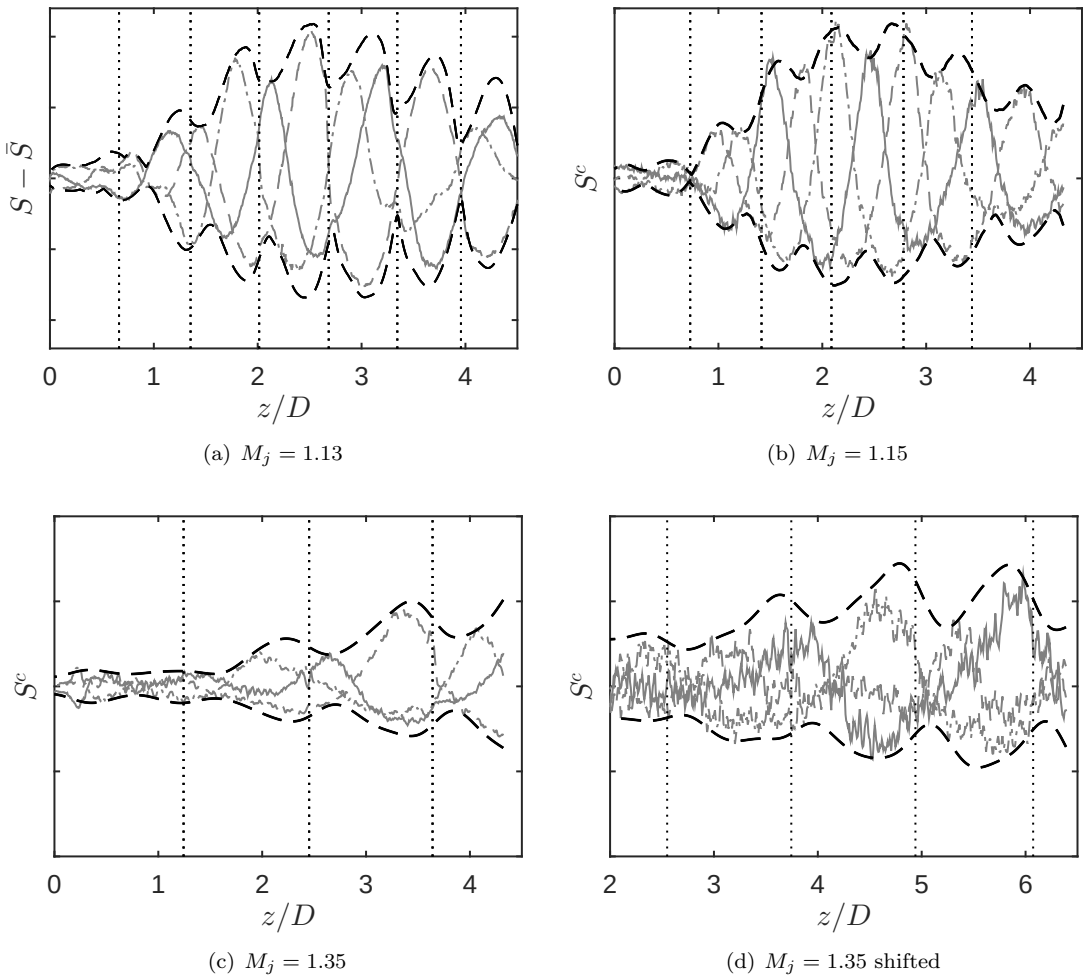

(a) $M_j = 1.13$ (b) $M_j = 1.15$

(c) $M_j = 1.35$ (d) $M_j = 1.35$ shifted

Fig. 4 Gray level $S^c(z, r/D = 0.5)$ of the result of the phase average for the three jets measured along the lip line, and after the full scope time average image is subtracted. The three gray lines ——, – – –, – · – correspond to three equi-spaced phases. The black dashed line – – – is the envelope computed from all available 45 (90 for older records) phases incremented by 8° (4°for older records). Vertical dotted lines indicate the shock locations.

in literature, for instance Powell,[3] Panda *et al.*[6] or Kerhervé *et al.*,[19] but results introduced in these studies consist of average values over a given extent in the axial direction. These velocity are found to be dependent upon the screech mode but most of them are comprised between $U_c/U_j = 0.65$ and 0.75. In order to build a feedback loop between the nozzle and the screech source, one needs to estimate the average convective velocity between these two points. This objective is reached here by determining the spatial evolution of the convective velocity along the shear layer.

A. Convective velocity estimation method

In an attempt of determining the convective velocity, the instability wave-number k_h resulting from large coherent structures is estimated from the measurement of the instability wave wavelength $\lambda_h = 2\pi/k_h$. The development of instability waves is assumed to start right downstream the nozzle. This origin also defines the reference point that will serve for the space time cross-correlation utilized to figure out instability wavelength. In effect, due to the periodic property of screech, the signal $S^c(z = 0,\ r = 0.5D)$ at the nozzle lip is expected to be in phase with the signal $S^c(z = n\lambda_h,\ r = 0.5D)$ measured at every location separated from the nozzle by an integer number n of period, thus wavelength. In practice, hydrodynamic contribution to the schlieren signal is far weaker than acoustic one at the nozzle lip. As a consequence, the reference signal is not dealing with hydrodynamic quantities but acoustic. However, if the acoustic wave triggers the hydrodynamic wave,

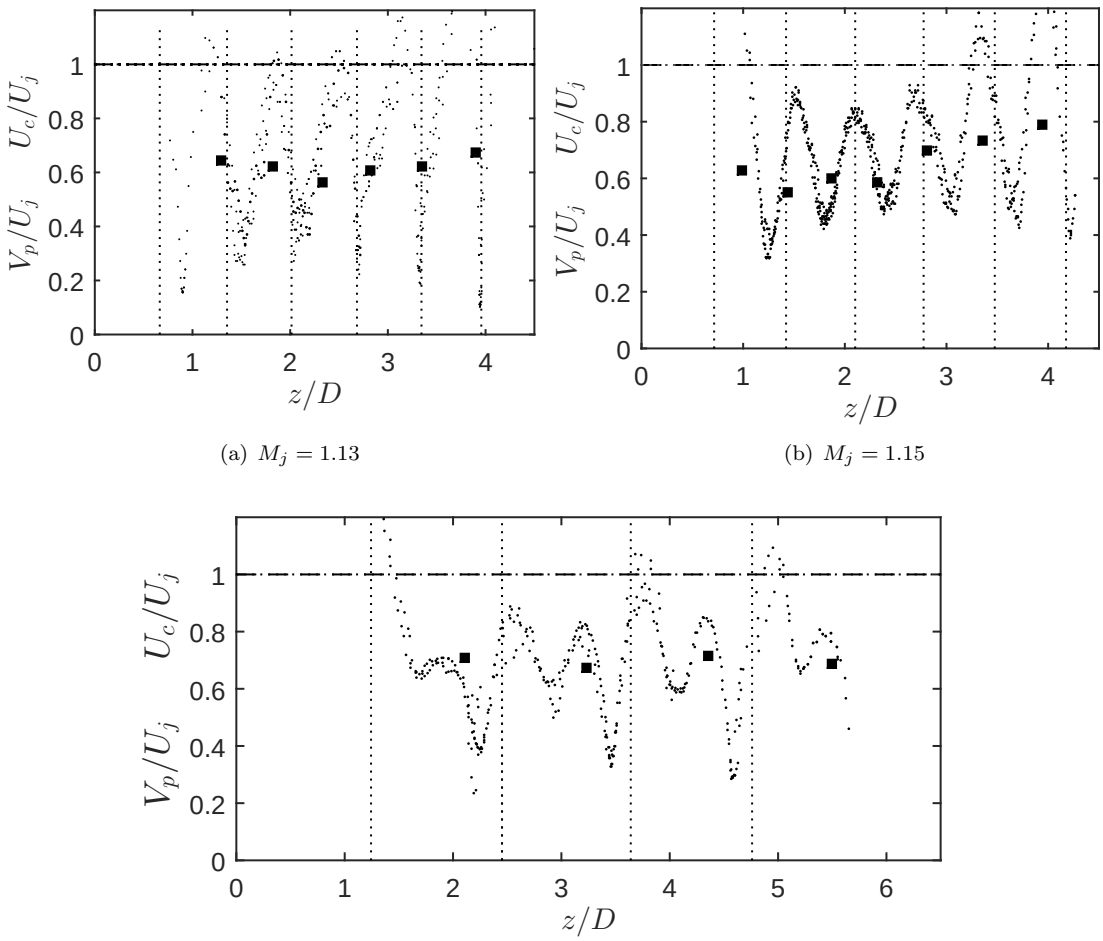

(a) $M_j = 1.13$ (b) $M_j = 1.15$

(c) $M_j = 1.35$

Fig. 5 Dots mark the hydrodynamic/acoustic phase velocity V_p estimation against the downstream distance from the nozzle. Black rectangles ■ correspond to the estimated structure convective velocities U_c. Velocities are normalized by the fully expanded jet exhaust velocity U_j. Vertical dotted lines indicate the shock locations.

both must be in phase and somehow related in terms of amplitude. Therefore, there is no difference in using acoustic instead of hydrodynamic as a phase reference.

The phase comparison between the nozzle attached reference signal and signals in the lip line is performed through the interpretation of the following cross-correlation function R normalized by standard deviations $\sigma_s(z)$

$$R(z,\tau) = \frac{\overline{s(z=0,t)s(z,t+\tau)}}{\sigma_s(z=0)\sigma_s(z)} \tag{5}$$

The filmed records are sampled at 220 kHz (or 430 kHz for older records), that is to say in the order of fifty to hundred times the screech frequency, even if screech is a few decades dB stronger than broad-band noise, the sample large bandwidth brings out such an amount of noise that the correlation between two points is lost over very short distance that never exceed $0.1D$. In this case, a pre-processing step is necessary to reduce the noise contribution to the signal. Time histories are then band-pass filtered with cut-off frequencies set at $\pm 6\%$ the screech frequency f_s by an IIR Butterworth fourth order filter.

After filtering, signals of both the reference and the moving points are divided into equal sections of duration $1.1T_s$ without overlap. Cross-correlation functions are then computed successively from all the sections. They are in the form of cosine decaying when τ get away from 0. Because the time sections used for the cross-correlation are equal to $1.1T_s$, only one complete period of this cosine is visible in both the positive

lag and negative lag semi-planes. The ten more percent of screech period are used to ensure that at least one screech period is covered even if the frequency drifts over the experiment. Now, only the positive lag semi-plan is considered and the lags corresponding to the higher local maximum (means sign inversion of the slope) and to the lower local minimum are recorded. This lag measurement is repeated for all the cross-correlation functions computed from all sections. The average lags of the local maxima and minima are computed for each point of the the lip line and reported against the location of the moving point used for the cross-correlation. The result is given in figure 6 in which lags of the maximum of the positive part of the cross-correlation function are represented by the solid line, whereas lags of the minimum are the dashed line. It is to be noted that the maximum lag never reaches a full screech period, and the minimum never reaches zero. This is due to averaging effect because the screech cycle is not exactly the same in all time sections, and the jump in lag from T_s to 0 is moving. This is also why the jump occurs over few points whereas the same figure obtained from a unique section of the record is characterized by jumps from T_s to 0 over only one z increment.

Equation 5 is used for treating the data in which the nozzle is visible, however when the field view is shifted for $M_j = 1.35$, the reference point to be considered is $z = 3.8D$. In effect, any location at which lag is zero is in phase with the $z = 0$ reference, and is eligible to be another reference location that is expected to show out same results. The zero lag at $z/D = 3.8$ is visible on the two records, and is therefore used as reference point for the axially shifted record. Results of both records can be compared in the overlap region in figure 6(c), and are found to be similar. This comparison confirms the validity of the second point of reference. From the maxima curve, the jumps in lag can be interpreted as the location of the end of the previous wavelength and the begin of the next, then the distance between two jumps is the wavelength. The minima curve gives details on the mid point of structures because a jump represents the location of two signals in opposition of phase. Thus, considering maxima and minima curves together, the length between two jumps is equal to the half wavelength of the local structure, and since the local hydrodynamic wave-number $k_h = 2\pi f_s/U_c$, the convective velocity is

$$U_c = \lambda_h f_s \tag{6}$$

The different behavior upstream and downstream a certain limit already identified as to be the receptivity region in Section B can be observed in figure 6. In this region, the phase velocity is pointing upstream because acoustic is predominant. As a consequence, to make both regions comparable in term of lag against axial location, in region where resultant wave is moving upstream, the negative lag semi-plane would be considered when sorting out maxima and minima of the cross-correlation function. This region contains information about acoustics, but is smaller than half a wavelength, so it is difficult to extract any result. Therefore, this region is finally disregarded.

B. Convective velocity analysis

The comparison between the convective velocity of the three modes is made in figure 7. It appears that mode A2 reaches the fastest speed with global increase between $U_j = 0.6U_c$ at $z/D = 2$ to $U_j = 0.8U_c$ at $z/D = 4$. B mode is a bit slower, its convective velocity oscillate between $U_j = 0.67U_c$ and $U_j = 0.7U_c$ from $z/D = 2$ to $z/D = 5.5$. Finally A1 mode experiences same behavior as A2 but reaches only $U_j = 0.67U_c$ at $z/D = 4$. Panda *et al.*[20] measured the averaged convective velocity of mode A2 equal to $U_j = 0.67U_c$ which is consistent with present estimations. Mode B is found faster than Panda *et al.*[20] and Massey and Ahuja[21] who measured respectively $U_j = 0.58U_c$ and $U_j = 0.60U_c$ against $U_j = 0.68U_c$ for the present study, this measurement is also sustained by another setting point at $M_j = 1.325$ not presented but that provide U_j varying between 0.65 and $0.71U_c$ over the same spatial range.

A limit of the present method is the poor spatial resolution. Convective velocity is indeed averaged over half a wavelength, and therefore is not able to describe phenomena such a modulation induced by shock-cells because both lengths are similar. Moreover, the location of structures boundaries is dependent upon the location of the reference point. To moderate this statement, if for some reason structures are not generated at the nozzle lip, there is no consequence on convective velocity, nevertheless location at which velocity is estimated is affected.

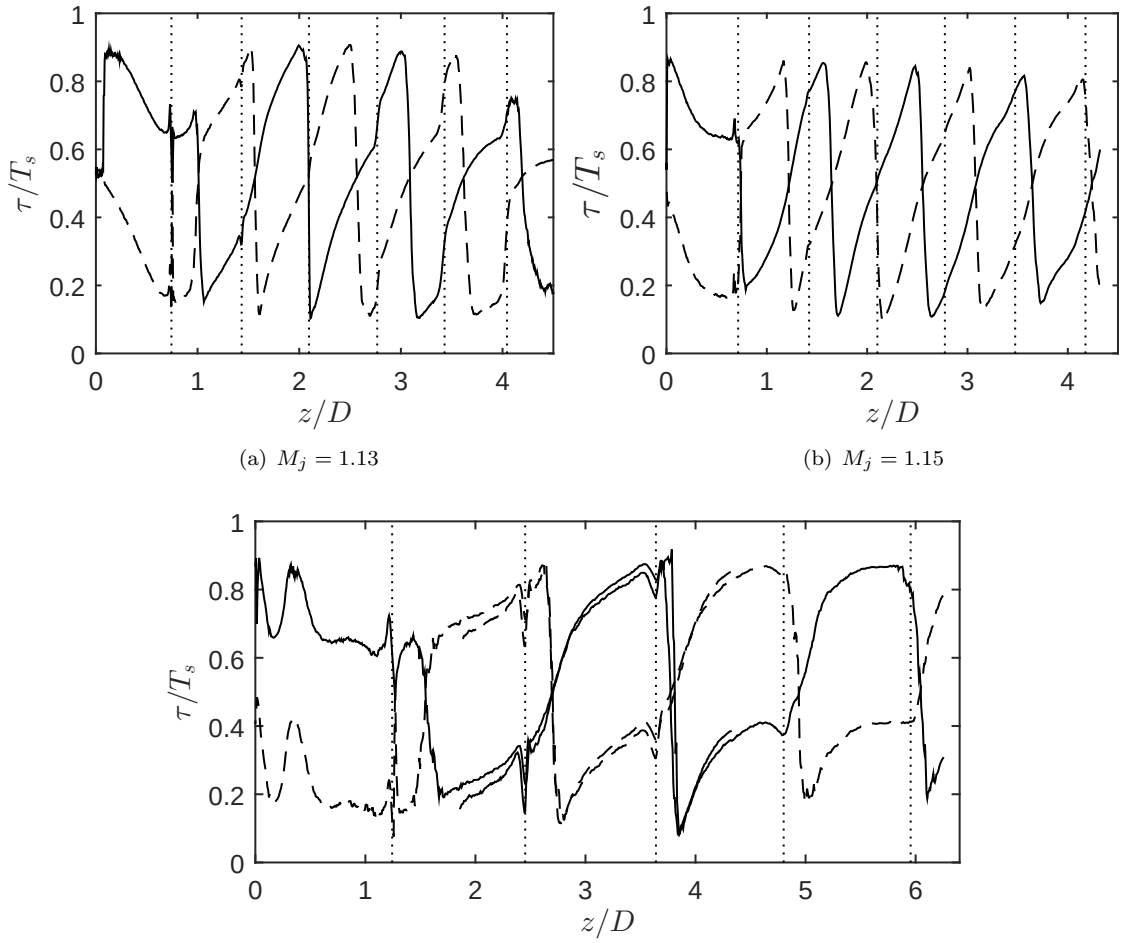

(a) $M_j = 1.13$ (b) $M_j = 1.15$

(c) $M_j = 1.35$

Fig. 6 Results deduced from the cross-correlation between a time history attached to the nozzle, and time histories of a moving point along the lip line $r/D = 0.5$. ——, lag of the maximum cross-correlation function at all moving point.– – –, lag of the minimum cross-correlation function at all moving point. Vertical dotted lines indicate the shock locations. For the case $M_j = 1.35$, the reference point of the right part is located at $z/D = 3.8$ instead of $z/D = 0$.

V. Source location identification

A. Screech loop consistency analysis

In this paragraph, the closure of the screech feedback loop is examined in the $(z/D, \phi)$ plane. The curves of the figure 6 are exploited as follow: first, considering the solid line, for each falling edge crossing $\tau/T_s = 0.5$, the axial position z/D is noted and the associated phase is a multiple of 2π. This result is then reported in the figure 8. In the same way, for dashed curves in figure 6, the location of each falling edge is plotted in figure 6 with the phase being an odd multiple π. These points are linked together in the figure 8 so as to constitute the hydrodynamic screech wave. On the graph, the shock positions are marked by the vertical dotted lines. An acoustic wave is supposed to be emitted at each intersection between these vertical lines and the screech wave. The acoustic wave is represented by straight line characterized by a slope of $-2\pi/\lambda_s$ where λ_s is the acoustic wavelength. In a first approximation, the wavelength is calculated for a constant speed of sound. According to the premise that an integer number of periods must be contained within the screech mechanism loop, only shock associated with cycles crossing $z/D = 0$ at an even number of π are able to constitute a convincing source for screech feedback.

Whatever the case, the arrivals of acoustic waves are not in phase and the feedback loops are never closed by

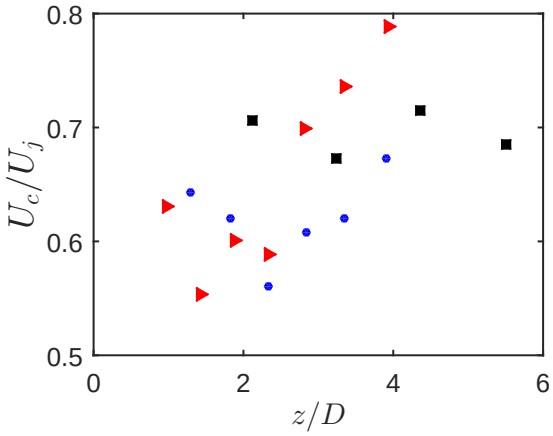

Fig. 7 Convection velocity normalized by the perfectly expanded jet speed along the axial direction. • $M_j = 1.13$, ▶ $M_j = 1.15$,■ $M_j = 1.35$

a multiple value of 2π. This indicate needs for further analysis, carried out here using nearfield microphones.

B. Near field acoustic

Two series of measurements have been conducted in order to clearly identify the screech acoustic source location. Both rest upon the synchronous use of two microphones, one stays steady while a second is moved point to point. In each case the aim is to compare the phase lag between each other with the phase lag theoretically found if a monopole was radiating at a shock tip such as $\Delta\phi = k_s(R - R_0)$, where R is the distance between the source and the moving microphone, and R_0 is the distance between the source and the reference microphone. Then, when experimental and expected phase lag are matching, the source is found. This kind of analysis provided Raman[7] with location of the source for rectangular screeching jets. This protocol is sketched in figure 9.

The first test consists in moving the microphone longitudinally at constant r. The fixed microphone lays at $r = 90$ mm ($r = 2.36D$) from the lip line and at $z = 14$ mm ($z = 0.37D$) from the nozzle end. The other microphone is at constant $r = 1D$ from the lip line and covers at least the first six shocks. The second test is a radial traverse in the nozzle exit plane ($z = 0$ mm) from $r = 0.5D$ to $r = 8D$. The fixed microphone is 70 mm upstream the nozzle and 70 mm away in radial direction, it is part of the plane defined by the jet axis and the moving microphone.

The radial traverse takes advantage of the very low hydrodynamic pressure field close to the nozzle, the processing is therefore straightforward and the phase lag is directly measured from cross-spectrum. Experimental results are comparable to expected radial phase lag evolution without offset problem. The best agreement between experimental and theoretical results is found when the the fourth shock tip is considered as source. The solid line in figure 10 is the result provided by the model for this source position. Furthermore, an example is provided for the case $M_j = 1.15$ with the third shock as source in dashed line, and the fifth shock in dash-dotted line. One will note that agreement is better at low r than higher. This might be explained by the progressively reducing amplitude of screech while broad-band shock associated noise is increasing. An example of spectrum corresponding to $2D$ to $8D$ is given in figure 11, for $M_j = 1.13$.

The processing of the results obtained from longitudinal investigation requires treatments more complicated than obtaining the phase difference from the cross-spectrum between the fixed and the moving microphones. The contribution of strong hydrodynamic fluctuations to the near field fluctuating pressure makes difficult interpreting spatial phase evolution directly deduced from cross-spectrum. It is not straightforward to distinguish the unexpected phase jumps involved by the two traveling wave interactions from the 2π indeterminacy. As a consequence a treatment similar to the phase velocity estimation was chosen. The signal of the fixed microphone is bandpass filtered. Then in the same way as it is explained in Section 2, each screech periods of the record is delimited from location of maxima in the reference time history. All periods of the record are then discretized into twenty sections equal in length that correspond to twenty

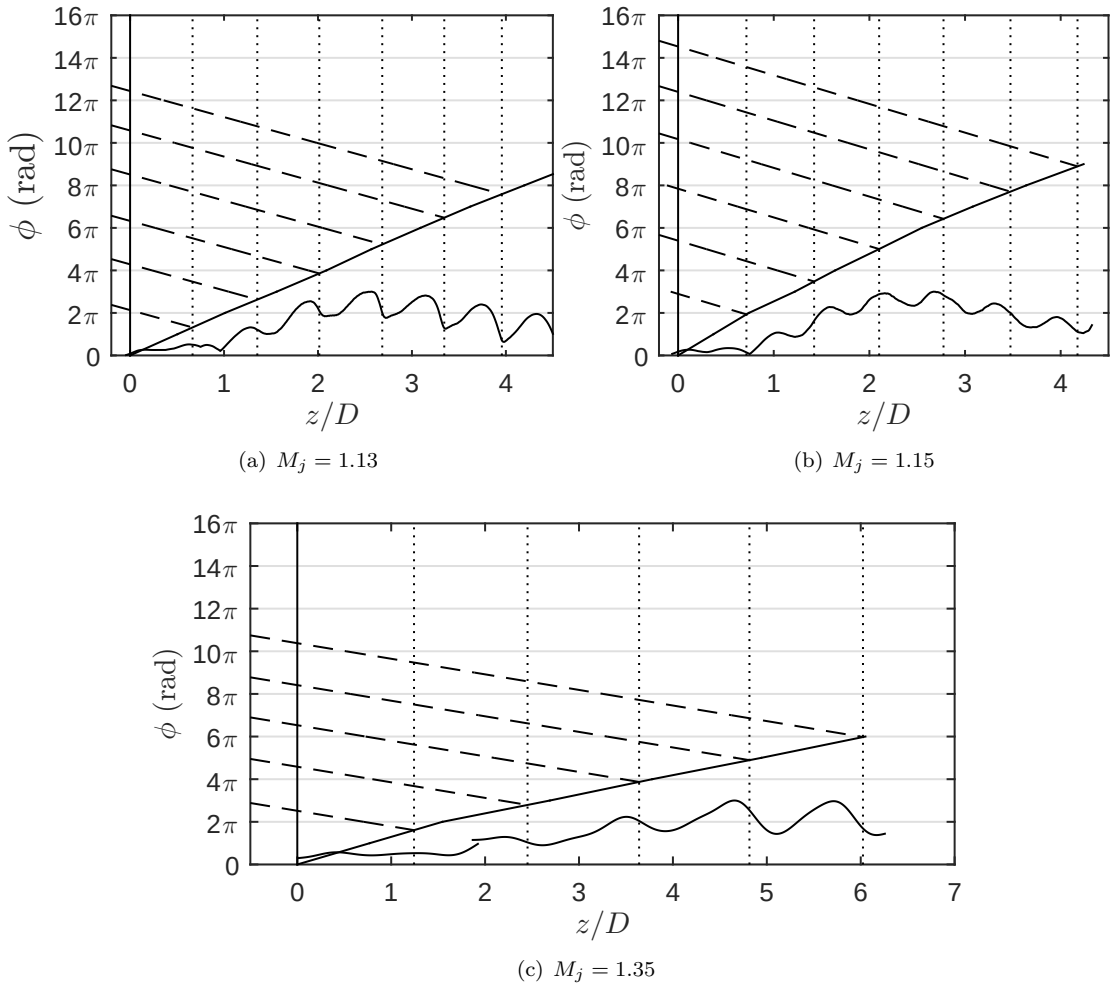

(a) $M_j = 1.13$

(b) $M_j = 1.15$

(c) $M_j = 1.35$

Fig. 8 Representation of the screech loops. The solid line represents the hydrodynamic screech wave, the dashed lines represent the acoustic feedback. The vertical dotted lines marks the shock positions. The curve line is the upper envelope of the stationary wave deduced from the phase average analysis

increments of phase in a screech period. All the samples of the moving microphone record that are in the same section, thus in phase, are finally averaged. This process is repeated for all longitudinal locations of the experiment. The spatial wave is then rebuilt for each phase since at all location, phase averaged signals are in phase with the reference microphone. An example at $M_j = 1.13$ of the amplitude p of the phase averaged acoustic wave against the axial location z/D of three acoustic waves is presented in figure 12 and corresponds to instant spaced by 126° in phase. The zero-crossing location of the wave are marked by a red dot if it is a raising edge or by a blue dot of it is a falling edge. The locations of these zero-cross dots are then reported against their respective phase in figure 13. This representation shows out curved line patterns that correspond to wavefronts which are propagating. It is to be noted that the acoustic feed back spends more that one period to reach the nozzle from the source. Therefore it has been chosen to perform the phase averaging over two consecutive periods in order to avoid any discontinuities along at least one wavefront. This implies that the final result is made of forty consecutive sections, and not twenty as if only one period were treated. According to the direction of propagation of the wavefront, either the red dot, or blue dot must be chosen so as to draw a pattern comparable with theoretical phase lag. In this case the leading edge of the waves is chosen, so red dot are chosen for wave that propagates upstream, and blue ones for wave that propagates downstream. The double arrow shows the two wave front that are visible in figure 14 (a). Results for the three cases are presented in figure 14. It is to be noted that the phase is arbitrarily set to 0 rad at $z/D = 0$.

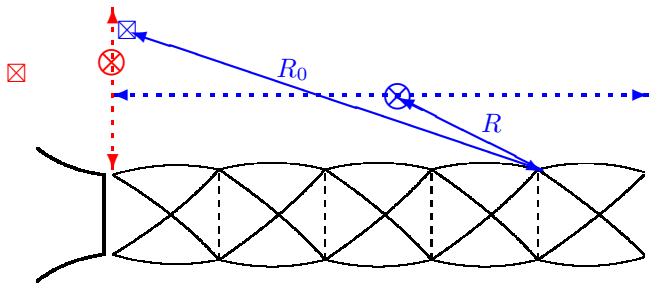

Fig. 9 Diagram describing the two traverse directions. ⊗ is for moving microphones, the blue one moves longitudinally across the blue dashed arrow, the red one moves radially across the red dashed arrow, they are associated with the corresponding reference microphones represented by ⊠

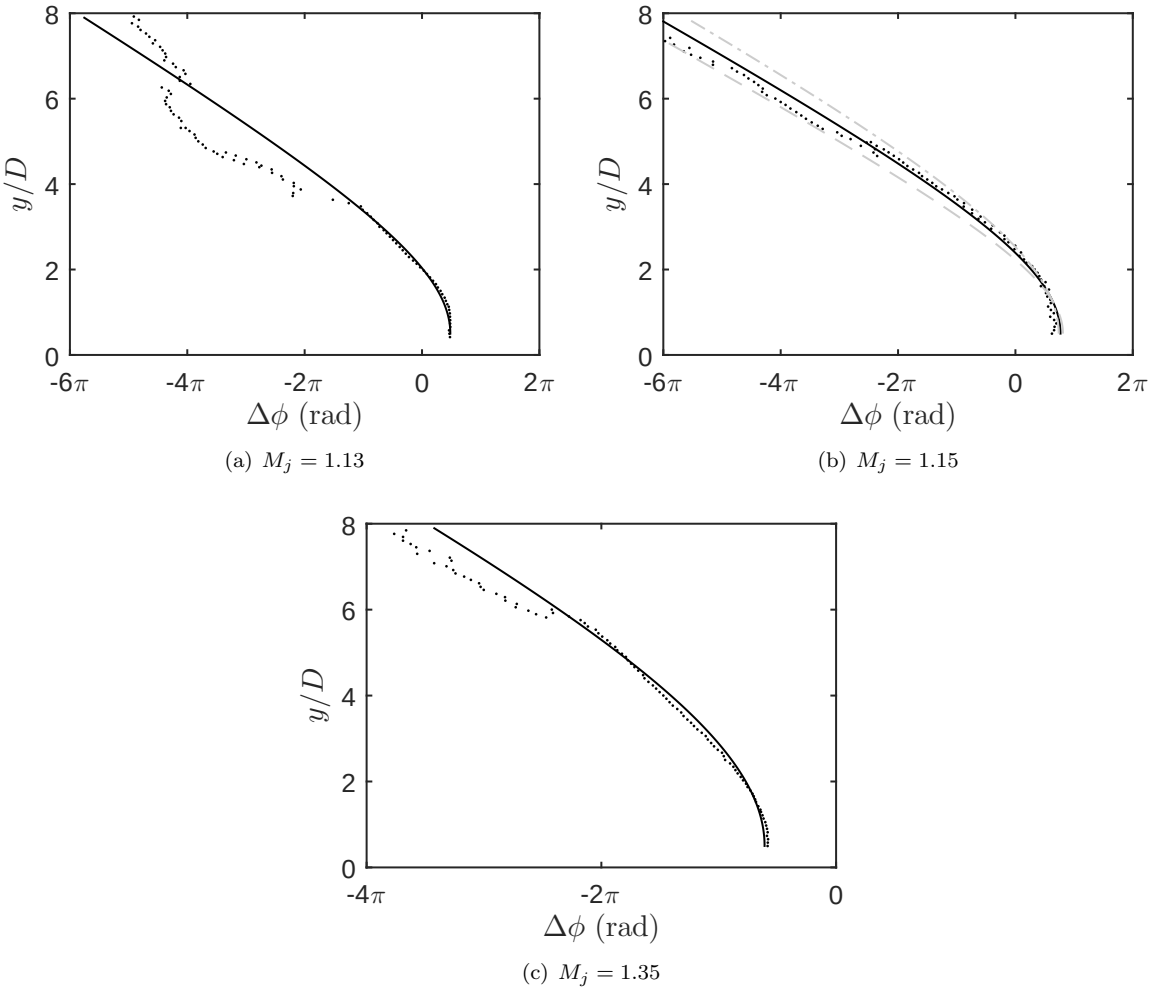

(a) $M_j = 1.13$

(b) $M_j = 1.15$

(c) $M_j = 1.35$

Fig. 10 Relative phase $\Delta\phi$ between the fixed microphone and the microphone traversing radially at constant $z/D = 0$. Dots represent experimental points, the solid line is the result from a model based on a single radiating monopole at the fourth shock tip. dashed and semi-dashed lines represent respectively results from the model with source located respectively at the third and fifth shock tip.

The adverse effect of the hydrodynamic fluctuations on relative phase measurement will be weakened in further experiments in which the distance between the jet and the moving microphone will be increased.

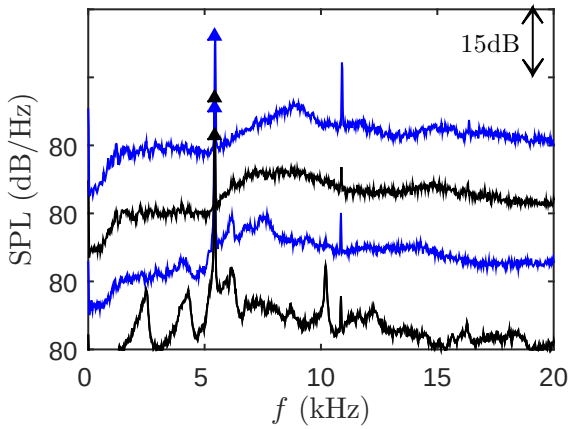

Fig. 11 Power spectrum density of measured fluctuating pressure on the jet $M_j = 1.13$ at $z/D = 0$, and from bottom to top at $r/D = 2, 4, 6, 8$. Triangles mark the maximum level at screech frequency for all the four locations and appear in the same order.

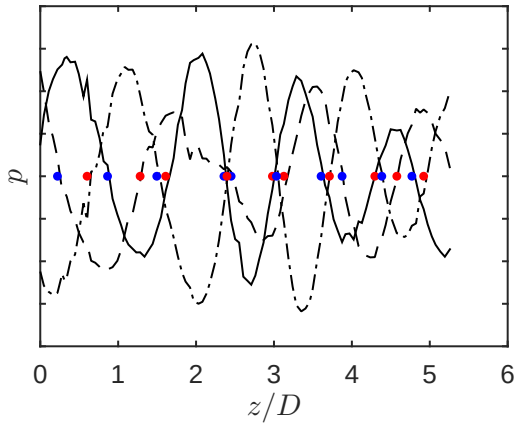

Fig. 12 Result of the phase averaged treatment on longitudinal nearfield acoustic. The solid line, then the dashed line and finally the dash-dotted lines represent the phase averaged acoustic wave at three instant spaced by about $2\pi/3$. • raising edge zero cross, • falling edge zero cross

C. Discussion

Near field acoustic measured through radial and longitudinal traverses tends to point out a best agreement between experimental and theoretical when the fourth shock is selected as source. Only the theoretical results derived from this source are shown for $M_j = 1.13$ and $M_j = 1.35$. Otherwise for $M_j = 1.15$, theoretical phase is exhibited with third, fourth and fifth shock as source. The sensitivity to the source axial location is fairly weak when only the radial results are considered, but a noticeable discrepancy comes out with increasing the phase ϕ when the source is the third or the fifth shock. Longitudinal traverses provide more sensitive results, but show out a behavior that does not agree well with the single monopole model downstream the source. Near this region, the amplitude of the standing wave envelope represented in figure 8 is maximum. It means the hydrodynamic pressure field is strong, therefore, the combination of the hydrodynamic and acoustic waves propagating in the same direction might result in a resultant wave traveling at higher phase velocity, hence involving a sharper phase increase.
Since the fourth shock is identified as the screech source, it is possible to isolate this path in figure 8, and to note that for all three modes, the feedback cross $z/D = 0$ just above an even number of π. Some error

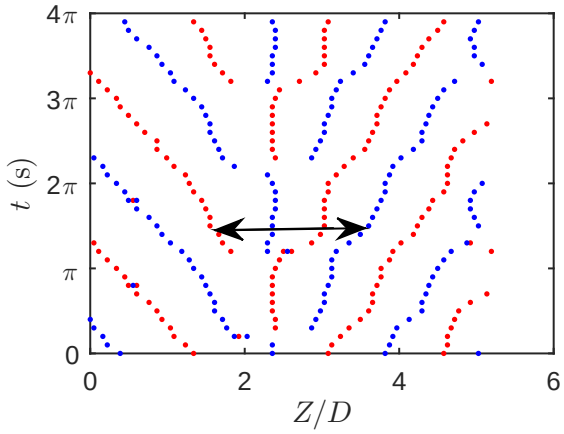

Fig. 13 Zero-crosses of the wave from the phase averaged treatment on longitudinal nearfield acoustic represented against their location, and phase in the screech cycle. • raising edge zero cross, • falling edge zero cross. The arrow indicates the wavefront associated pattern that is selected for the comparison with theoretical relative phase.

M_j	$\phi_{4^{th}}$ (rad)	$z_{4^{th}}$ (mm)	U_c (m/s)	U_c/U_j
1.13	16.4	102	210	0.60
1.15	20.2	106	203	0.57
1.35	15.4	183	244	0.60

Tab. 2 Screech associated structure convection velocity averaged between the nozzle and the fourth shock

on convective velocity estimation, and in particular if it was overestimated, would justify this disagreement with the hypothesis that the zero cross must be observed at an integer number of screech period.
Finally the mean convective velocity from the nozzle to the fourth shock is likely to be estimated since the time a structure spends to reach the shock from the nozzle is deduced in accordance with results shown in figure 8. The convective velocity U_c is

$$U_c = f_s \frac{2\pi}{\phi_{4^{th}}} z_{4^{th}} \tag{7}$$

where f_s is the screech frequency, $\phi_{4^{th}}$ is phase that a structure spends to reach the fourth shock from the nozzle, and $z_{4^{th}}$ is the coordinate of the fourth shock. The table 2 summarizes estimated convective velocity for the three cases, so for modes A1, A2, and B. The convective velocity is found equal for mode A1 and B, and 5% lower for mode A2. Those results are all lower than that presented in Section 4 because the average is not performed on the same domain. Convective velocity of jets at $M_j = 1.13$ and $M_j = 1.15$ is still increasing downstream the fourth shock. Moreover, large eddy simulation results for an undexpanded $M_j = 1.56$ screeching jet led Gojon[22] to measure convective velocity equal to $0.35U_j$, which correspond to half the ejection velocity, right downstream the nozzle, and then reaches $0.65U_j$ two diameters downstream. No account is made of this low convective velocity in Section 4, hence these values are overestimated from screech feedback loop point of view.
The shift of frequency between mode A1 and A2 is not the result of an higher convective velocity. Nevertheless, examination of figure 8, and in particular at $z/D = 0$ points out that the feedback reaches the nozzle back after 8π for modes A1 and B, but 10π for the mode A2. There is therefore five distinct structures in the loop of mode A2 rather than four in the loops of modes A1 and B.

VI. Conclusion

The screech associated phenomena have been investigated with the aim of identifying its source location. The present post-processing procedure is based on the analysis of signals extracted from time-resolved

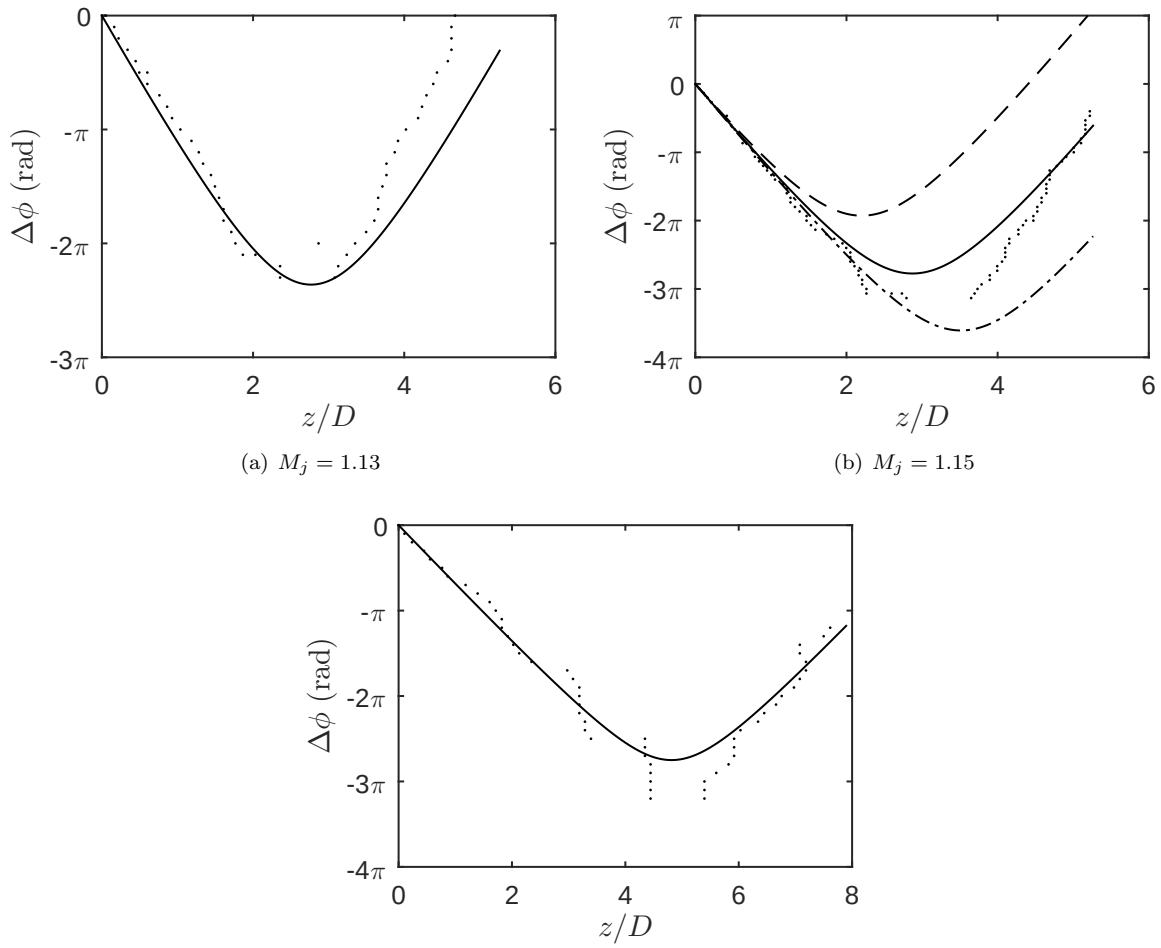

(a) $M_j = 1.13$

(b) $M_j = 1.15$

(c) $M_j = 1.35$

Fig. 14 Relative phase $\Delta\phi$ between the fixed microphone and the microphone traversing longitudinally at constant $r = 1.5D$. Dots represent experimental points, the solid line is the result from a model based on a single radiating monopole at the fourth shock tip. dashed and semi-dashed lines represent respectively results from the model with source located respectively at the third and fifth shock tip. Relative phase is arbitrarily set to zero at z/D=0

schlieren image data. The convection velocity can be estimated in the region where hydrodynamic overcomes acoustic, downstream a certain limit localized in the second shock cell. More generally, by using a phase average method, the phase velocity of the wave resulting from the interaction between hydrodynamic and acoustic can be determined. Finally, a representation of the screech loop is provided in the plane axial distance along the jet - phase to identify the most probable position of the screech sources. The screech loop consistency is also assessed by near field acoustic phase analysis. Noise sources are found located at the tip of the fourth shock whatever the mode is A1, A2 or B. Since the source is localized, it is possible to focus on the right screech loop. This screech loop is found to be composed of four screech periods for modes A1 and B, but five periods for mode A2. Similar results are currently established for various setting points for these modes.

Acknowledgments

This work was performed within the framework of the Labex CeLyA of Université de Lyon, within the program Investissements dAvenir (ANR-10-LABX-0060/ ANR-11-IDEX-0007) operated by the French National Research Agency (ANR), and is also partially supported by the industrial Chair ADOPSYS co-financed by SAFRAN-SNECMA and ANR (ANR-13-CHIN-0001-01).

References

[1]Tam, C. K., "Supersonic jet noise," *Annual Review of Fluid Mechanics*, Vol. 27, No. 1, 1995, pp. 17–43.

[2]Powell, A., "On edge tones and associated phenomena," *Acustica*, Vol. 3, 1953, pp. 233–243.

[3]Powell, A., Umeda, Y., and Ishii, R., "Observations of the oscillation modes of choked circular jets," *The Journal of the Acoustical Society of America*, Vol. 92, No. 5, 1992, pp. 2823–2836.

[4]Umeda, Y. and Ishii, R., "On the sound sources of screech tones radiated from choked circular jets," *The Journal of the Acoustical Society of America*, Vol. 110, No. 4, 2001, pp. 1845–1858.

[5]Tam, C. K., Parrish, S. A., and Viswanathan, K., "Harmonics of Jet Screech Tones," *AIAA Journal*, Vol. 52, No. 11, 2014, pp. 2471–2479.

[6]Panda, J., "An experimental investigation of screech noise generation," *Journal of Fluid Mechanics*, Vol. 378, 1999, pp. 71–96.

[7]Raman, G., "Cessation of screech in underexpanded jets," *Journal of Fluid Mechanics*, Vol. 336, 1997, pp. 69–90.

[8]Suzuki, T. and Lele, S. K., "Shock leakage through an unsteady vortex-laden mixing layer: application to jet screech," *Journal of Fluid Mechanics*, Vol. 490, 2003, pp. 139–167.

[9]Shariff, K. and Manning, T. A., "A ray tracing study of shock leakage in a model supersonic jet," *Physics of Fluids*, Vol. 25, No. 7, 2013, pp. 076103.

[10]Berland, J., Bogey, C., and Bailly, C., "Numerical study of screech generation in a planar supersonic jet," *Physics of Fluids*, Vol. 19, No. 7, 2007, pp. 075105.

[11]André, B., Castelain, T., and Bailly, C., "Shock-tracking procedure for studying screech-induced oscillations," *AIAA journal*, Vol. 49, No. 7, 2011, pp. 1563–1566.

[12]André, B., Castelain, T., and Bailly, C., "Broadband shock-associated noise in screeching and non-screeching underexpanded supersonic jets," *AIAA journal*, Vol. 51, No. 3, 2013, pp. 665–673.

[13]Gao, J. and Li, X., "A multi-mode screech frequency prediction formula for circular supersonic jets," *The Journal of the Acoustical Society of America*, Vol. 127, No. 3, 2010, pp. 1251–1257.

[14]Edgington-Mitchell, D., Oberleithner, K., Honnery, D. R., and Soria, J., "Coherent structure and sound production in the helical mode of a screeching axisymmetric jet," *Journal of Fluid Mechanics*, Vol. 748, 2014, pp. 822–847.

[15]André, B., Castelain, T., and Bailly, C., "Experimental study of flight effects on screech in underexpanded jets," *POF*, Vol. 23, No. 12, 2011.

[16]Westley, R. and Woolley, J., "The near field sound pressures of a choked jet during a screech cycle," *AGARD Conference Proceedings*, No. 42, 1969, pp. 23–1.

[17]Panda, J., "An experimental investigation of screech noise generation," AIAA Paper 96-1718, 1996.

[18]Mercier, B., Castelain, T., and Bailly, C., "Investigation of under-expanded jet screech associated convective velocity based on high frequency sampled schlieren visualisations," *22ème Congrès Français de Mécanique*, 2015.

[19]Kerhervé, F., Jordan, P., Gervais, Y., Valière, J.-C., and Braud, P., "Two-point laser Doppler velocimetry measurements in a Mach 1.2 cold supersonic jet for statistical aeroacoustic source model," *Experiments in fluids*, Vol. 37, No. 3, 2004, pp. 419–437.

[20]Panda, J., "Underexpanded Screeching Jets From Circular, Rectangular, and Elliptic Nozzles," .

[21]Massey, K. C. and Ahuja, K. K., "Screech frequency prediction in light of mode detection and convection speed measurements for heated jets," AIAA Paper 97-1625, 1997.

[22]Gojon, R., Bogey, C., and Marsden, O., "Large-eddy simulation of underexpanded round jets impinging on a flat plate 4 to 9 radii downstream from the nozzle," AIAA Paper 2210-2015, 2015.